YJFLS: 103758

ARTICLE IN PRESS

Journal of Fluids and Structures xxx (xxxx) xxx

Contents lists available at ScienceDirect

Journal of Fluids and Structures

journal homepage: www.elsevier.com/locate/jfs

Generalized lift force model under vortex shedding

François Rigo [a,b,c,*], Thomas Andrianne [a], Vincent Denoël [c]

[a] Wind Tunnel Lab, University of Liège, Belgium
[b] FRS-FNRS, National Fund for Scientific Research, Liège, Belgium
[c] Structural & Stochastic Dynamics, University of Liège, Liège, Belgium

ARTICLE INFO

Article history:
Received 1 March 2022
Received in revised form 30 August 2022
Accepted 11 September 2022
Available online xxxx

Keywords:
Vortex shedding model
Circular cylinder
Wind tunnel experimental testing
Lift coefficient
Non-linear oscillator
Wake-oscillator

ABSTRACT

This paper proposes a generalized model for vortex shedding around a static cylinder. This model is a first step to bridge the gap between two existing families of Vortex Induced Vibration (VIV) models , namely (1) stochastic spectral models and (2) wake-oscillator models with coupled fluid and structural equations. The first family is experimentally-based while the models of the second family typically rely on theoretical and phenomenological concepts. These models use a Van der Pol, Rayleigh or a combination of both oscillators for the lift equation. The proposed model generalizes these models by combining all third degree terms in the case of a static model, i.e. by considering the equation of the fluid oscillator only. It is possible to enrich existing models with a more complex parametric model because its parameters are identified from experimental data. A second specificity of the proposed model stems from the observation that, for a static cylinder in low turbulence flow, the envelope of the measured lift force is not perfectly mono-harmonic, nor deterministic. Turbulence in the wake is expected to create fluctuations in the lift envelope. In the proposed model, stochasticity is consequently introduced to reproduce these fluctuations. It is based as an additive exogenous noise as an input to the generalized shedding model, using a Von Karman spectrum. Its coefficients are adjusted so that the model reproduces the probability density function of the measured lift envelope (and its power spectral density). The methodology is applied to Wind Tunnel data of a static circular cylinder in subcritical and postcritical regimes. This set of data is used to identify the coefficients of non-linear terms and Von Karman spectrum. The lift fluctuation coefficient generated with the model matches results available in the literature for the considered regimes. This work focuses on a methodology to obtain a generalized vortex shedding model from experimental data measured on a static body. It can be applied to other cylinder cross-sections or even extended to cylinders arranged in tandem.

1. Introduction and motivation

At medium to high Reynolds number, the flow behind bluff bodies is separated with vortices ejected alternatively on both sides of the body. For symmetric geometries such as circular cylinders, vortex shedding creates a change in pressure distribution on both sides of the cylinder which creates an oscillating resulting lift force. According to the Strouhal law, the vortex shedding frequency varies linearly with the incoming fluid velocity. For flexible or rigid spring-mounted structures, once this frequency matches the natural frequency of the structure left free to vibrate, the coupling between

* Corresponding author at: Wind Tunnel Lab, University of Liège, Belgium.
E-mail address: francois.rigo@uliege.be (F. Rigo).

https://doi.org/10.1016/j.jfluidstructs.2022.103758
0889-9746/

both degrees-of-freedom (structure and fluid) leads to the resonance of the structure. This phenomenon is called Vortex Induced Vibration (VIV) and different models have been proposed in the literature. They can be classified into two groups according to the number of equations (one or two). Models (1.) focus on the structural equation, with different ways to take into account the flow loading on the second member of the equation : (1.i) a simple external harmonic excitation from the lift force, (1.ii) a lift force that depends on the structural velocity and/or acceleration, giving an equivalent damping model, (1.iii) a spectral model of stochastic loading to take into account turbulence. In the following, symbol (1) is used to refer to model (1.iii). Models (2) use a coupled differential system with two variables : the structure and the wake. These models highlight the importance of considering the flow as a variable with its own equation that interacts with the structure and not a simple forcing term.

In Model (1.i), the lift force on a static circular cylinder is represented using a harmonic loading. Nevertheless, experimental data show that the lift is not perfectly harmonic, even for uniform (or low turbulence) fluid velocity (Collins, 1976; Huseby and Grue, 2000). Indeed, Bishop and Hassan (1964) showed high fluctuations in the measured lift envelope for a circular cylinder without end-plates. They showed non-negligible fluctuations even with end plates, which suggested that in addition to three dimensional effects along the short span tested specimen, turbulence can develop in the boundary layer and in the wake. The modelling of forces resulting from the flow around static cylinder and their fluctuating behaviour is part of the motivation of this work.

When the structure is static, models that take into account only the structure (models (1.i-ii)) cannot simulate the fluid behaviour. Model (1) is able to represent the fluid alone with a spectral formulation. Models (2) without structural motion simplify into one equation for the fluid. In this context, models describing the flow around static cylinders can be finally classified into two families : (1) data driven or empirical (Vickery and Clark, 1972; Vickery and Basu, 1983; Basu and Vickery, 1983) (spectrum) and (2) non-linear models such as the wake-oscillator (Tamura, 1981; Facchinetti et al., 2004). The first family includes the well known Vickery–Basu model (Vickery and Clark, 1972; Basu and Vickery, 1983) and refers to experimentally-based models to obtain, directly, the spectrum of the lift force. They capture the frequency content around the vortex shedding frequency but fail to represent other frequency ranges. The lift is a narrow-banded process.

In this paper, focus is on the flow and resulting lift force on a static (fixed) cylinder. The dynamic of the lift coefficient is captured by a single non-linear equation : the second equation of a wake-oscillator model.

Existing wake-oscillator models are deterministic and aim to replicate the synchronization features observed in experiments. They are mainly used today to provide the steady state response, which corresponds to harmonic or quasi-harmonic response in most cases. Some of them are reviewed next.

Tamura's model (Tamura, 1981) hinges on a Van der Pol type equation for the wake variable α (angle of the wake lamina). It is theoretical and based on physical principles to model the wake lamina as a torsional oscillator. Tamura's model, applied on a static cylinder ($y = 0$), leads to a lift coefficient given by $C_L = -f\alpha$, where

$$\ddot{\alpha} - 2\xi_f \Omega \left(1 - 4\frac{f^2}{C_{L0}^2}\alpha^2\right)\dot{\alpha} + \Omega^2\alpha = 0. \tag{1}$$

The meaning and values of model parameters f, ξ_f, C_{L0}, Ω are discussed in the original paper (Tamura, 1981). For a static cylinder, the frequency is equal to the vortex shedding frequency and the frequency ratio $\Omega = 1$. By substituting $q = \frac{2f}{C_{L0}}\alpha$ and $\varepsilon_T = 2\xi_f$ (equivalent fluid damping), $C_L = \frac{C_{L0}}{2}q$, it can be written,

$$\ddot{q} - \varepsilon_T(1 - q^2)\dot{q} + q = 0. \tag{2}$$

In a similar way, Hartlen and Currie (1970) used a Rayleigh-type equation for the fluid degree of freedom to model VIV. For a static cylinder ($y = 0, \Omega = 1$), their model reads

$$\ddot{C}_L + (g\dot{C}_L^2 - a)\dot{C}_L + C_L = 0 \tag{3}$$

with the symbols g, C_L, a of the original paper (Hartlen and Currie, 1970). By substituting original parameter values $\varepsilon_H = a = 3gC_{L0}^2/4$ and $C_L = \frac{\sqrt{3}}{2}C_{L0}q$, the governing equation becomes

$$\ddot{q} - \varepsilon_H(1 - \dot{q}^2)\dot{q} + q = 0. \tag{4}$$

Krenk and Nielsen (1999) used quadratic damping and an energy-based model. It corresponds mathematically to a combination of Van der Pol and Rayleigh equations. For a static cylinder ($y = 0, \Omega = 1$) and by substituting $q = w/w_0$ and $\varepsilon_K = 2\xi_f$, in his original model, the equation governing the dynamics of shedding reads

$$\ddot{q} - \varepsilon_K\left(1 - \left(q^2 + \dot{q}^2\right)\right)\dot{q} + q = 0 \tag{5}$$

with $C_L = \frac{\dot{w}}{U}\gamma = \frac{\dot{w}}{w_0}C_{L0} = C_{L0}\dot{q}$. The main difference between Krenk's and the previous models is the link between the wake variable q and the lift C_L, with a derivative $\dot{q} = C_L/C_{L0}$, that comes from an energy-based model. Mathematically, these three equations exhibits a similar structure : they possess a limit cycle and are able to model the experimental feature of vortex shedding, in particular the self limitation of the phenomenon. All these models can be cast in a generalized form

$$\ddot{q} + q = F(q, \dot{q}) = \dot{q}(\alpha q^2 + \beta q\dot{q} + \gamma\dot{q}^2 + \delta) \tag{6}$$

Table 1
Coefficients of non-linear terms of wake-oscillator general models.

	α	β	γ	δ
Tamura	$-\varepsilon_T$	0	0	ε_T
HC	0	0	$-\varepsilon_H$	ε_H
Krenk	$-\varepsilon_K$	0	$-\varepsilon_K$	ε_K

where coefficients $\alpha, \beta, \gamma, \delta$ take different values for each model, see Table 1. None of these models uses β, which is shown later to not contribute to the lift envelope.

It is likely that these models are kept in a minimalistic formulation by their authors, so as to keep them simple and a main argument explaining their usage is that they show the features of vortex shedding. From a comparison with a detailed wind tunnel analysis, additional terms of Krenk's model allowed more versatility and showed better accuracy (Krenk and Nielsen, 1999). However, we notice that the three remaining parameters α, γ, δ of Krenk's model are all express according to the same unique quantity, ε_K.

By keeping the general formulation of Eq. (6), with α, γ, δ possibly different, we further increase the range of possible dynamics spanned by the model, even if the term $\beta q\dot{q}^2$ will be dropped in the proposed model. In the subsequent approach, the parameters of the model are fitted to experimental data with the constrain to provide a limit cycle, characteristic of vortex shedding, but also to capture accurately both the fast and slow dynamics of the wake.

In doing so, we propose a data-driven model, while existing ones are theoretical (Tamura, 1981) or phenomenological (Krenk and Nielsen, 1999; Hartlen and Currie, 1970). To the author's knowledge, this work is the first identification of the non-linear coefficients of a loading model such as Eq. (6), based on experimental data and their dynamics, which is usual for model (1) but new for model (2).

Existing wake-oscillator models are deterministic and show harmonic or quasi-harmonic response in the steady state regime. However, experimental evidences show fluctuations in the lift envelope as introduced before. Eq. (6) is thus not sufficient and a randomization of this generalized model is therefore necessary. Such a randomization has been suggested in Denoël (2020) in the context of stochastic Vortex Induced Vibration (VIV) by adding a term $(1 + I_u)$ in front of U_∞, to study the influence of turbulence intensity and length scale on VIV using a randomized version of Facchinetti's model (another model based on Van der Pol equation). Nielsen and Krenk (1997) also studied a stochastic version of their energy balanced model for VIV by replacing the fluid velocity with $(1 + R(t))U_\infty$, with the turbulence represented by a non-dimensional stochastic process $R(t)$. Ulveseter et al. (2017) proposed to add a stochastic process on frequency so that the frequency of the vortex shedding force may vary in time, and the variation depends on the response of the structure. Aswathy and Sarkar (2019) introduced also a noisy fluid velocity input in simulations. So et al. (2008) studied the effect of free-stream turbulence on VIV of circular cylinder by adding turbulence grids. The incoming turbulence breaks partially the vortex shedding, which reduces the lock-in range and displacement amplitude but also feeds energy to the cylinder motion. It is believed that these stochastic models where the fluid velocity U is corrupted by noise are appropriate to model turbulence in the oncoming flow. Stochasticity in the envelope response is observable experimentally, though, even in case of uniform flow. Fluctuations in the lift are coming from variations in the boundary layer, wake turbulence and three-dimensional effects along the span. In this context, we chose to randomize the deterministic generalized model (6) with an additive noise which aims at capturing the turbulence in the near wake, a mechanism manifesting a different source of randomness than that resulting from the oncoming flow. A realistic frequency content for this additive term, interpretable as near wake (3D) turbulence, is then adjusted on experimental data in order to reproduce the spectrum of the lift.

Another specificity of this work is therefore to combine the non-linear model (6) with a stochastic approach, in order to model the randomness of the fluctuating lift envelope, even in uniform flow configurations. In some sense, the proposed procedure adds the "missing piece" between data-driven, theoretical and phenomenological models, including stochastic effects. This work can be seen as an effort to combine the advantage of two families of modelling : the stochasticity introduced by spectral method and the self-limiting nature of wake-oscillator models. We show in this paper that the proposed model is able to generate data, that are the closest to experimental measurements. It is done by firstly adjusting a deterministic generalized model and secondly adding the turbulent content that allows to reproduce the fluctuations of experimental data.

This paper is organized as follows. In Section 2, experimental data are presented. In Section 3, the deterministic part of the generalized model is introduced, with its main parameters. The proposed additive noise is then presented and the procedure to adjust its parameters is detailed. Results are shown in Section 4 and compare the present model with others to the experimental results, in terms of lift coefficient (complete signal and envelope) statistics : Probability Density Function (PDF) and Power Spectral Density (PSD). All coefficients and parameters (from the deterministic model and the additive noise) are discussed in term of flow regimes. The final output is a comparison of the lift fluctuations predicted by the model with literature results.

Table 2
Wind tunnel setup parameters.

Regime	Re	k/D
Sub1	$4.5 \cdot 10^4$	$4 \cdot 10^{-4}$
Sub2	$4.3 \cdot 10^4$	$7 \cdot 10^{-3}$
Post	$1.4 \cdot 10^5$	$7 \cdot 10^{-3}$

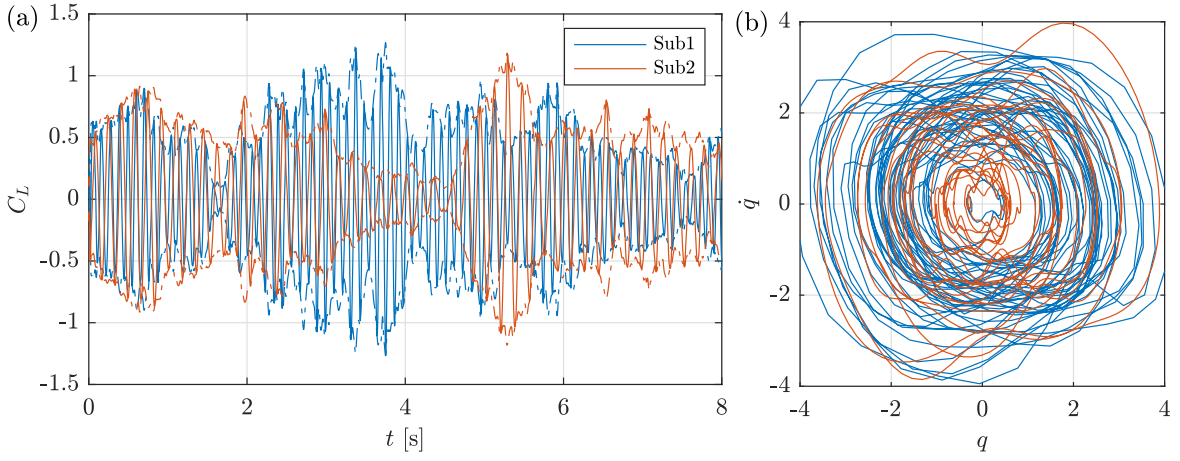

Fig. 1. Circular cylinder in subcritical regime : (a) experimental lift coefficient C_L and (b) its corresponding phase portrait $(q, \dot{q})$ with $q = \frac{2C_L}{C_{L_0}}$.

2. Experimental data

The parameters of the proposed generalized vortex shedding model are identified from experimental measurements. Pressure measurements are performed on a static cylinder in the Wind Tunnel Laboratory of University of Liège. The lift coefficient is obtained by integration from 46 unsteady pressure taps equally spaced around the mid-span section of a circular cylinder (span $L/D = 10$, with $D = 0.1$m the diameter of the cylinder and a blockage ratio in the WT test section of 3.3%). The data sets have been measured in uniform flow (turbulence intensity $I_u = \sigma_u/U < 0.2\%$) using a sampling frequency $f_s = 250$ Hz. Reynolds numbers covered subcritical and postcritical regimes and two surface roughnesses were investigated (with k/D the relative roughness). The complete set-up description can be found in Dubois and Andrianne (2022). The proposed methodology was applied to three types of flow, two subcritical and one postcritical, see Table 2. Labels (Sub1, Sub2, Post) will be used to identify regimes in the following discussion. The complete data set contains three Re for each regime and will be used in Section 5 to compare all identified coefficients. Meanwhile, some representative data sets are used to motivate and illustrate the derivation of the proposed model.

Fig. 1 shows samples of measured lift coefficient in subcritical regime around the smooth and the rough cylinder (Sub1 and Sub2). Despite the very low oncoming turbulence intensity ($I_u < 0.2\%$), variations in the envelope are observable. The lift is far from a harmonic or quasi-harmonic response, as also illustrated in the phase portrait $(q, \dot{q})$. For a perfect sine, the phase portrait would be a circle. The shape of the limit cycle is different here and oscillates around a limit cycle of amplitude around 2. These variations come from the generated turbulence in the boundary layer around the cylinder and in the wake. Three dimensional effects can also influence the size and ejection location of the vortices around the cylinder and along the span. The relation of the flow between two locations along the span of the cylinder is quantified in the coherence function. Turbulence effects are then also present in 3D space and not only in the 2D cross plane. From the time signal and phase portrait of the lift, the roughness seems to decrease the amplitude of these envelope variations but to accelerate their occurrence, i.e. faster dynamics, with a shorter characteristic time. Nevertheless, the shape of the phase portrait remains similar, suggesting similar non-linearities.

The envelope C_{L_e} represented by dashed lines in Fig. 1(a) is computed with the analytic signal of C_L, obtained with the Hilbert transform implemented in Matlab (2019). The probability density function (PDF) of the lift envelope C_{L_e} is illustrated in Fig. 2 for the three regimes. A mono-harmonic signal of constant amplitude (sine) would show a Dirac function for C_{L_e} at $\sqrt{2}C'_L$ (the root mean square (rms) of C_L).

It can be observed that $\mathcal{P}(C_{L_e})$ shows a similar shape for Sub1 and Sub2 cases, with a significant dispersion in C_{L_e}. Sub1 and Sub2 cases correspond to the subcritical regime, where Reynolds effects are very low and the flow exhibits a turbulent vortex street with a laminar boundary layer around the cylinder (Lienhard, 1966). Sub2 shows a higher cylinder surface roughness and the dispersion in C_{L_e} is slightly higher than the one for Sub1 case. In the critical regime, the laminar boundary layer undergoes a turbulent transition and no vortex street is apparent. The wake is disorganized. This regime

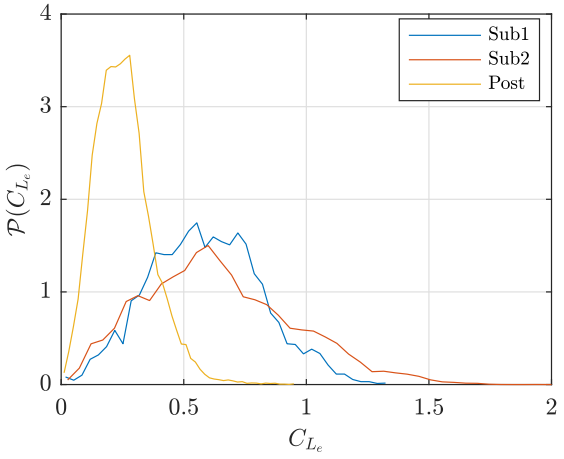

Fig. 2. Probability density function of the experimental lift envelope C_{L_e} for the different regimes.

is not studied here. The postcritical regime (Post) is characterized by a turbulent vortex street (re-established after the critical regime) and the boundary layer is turbulent. For this regime, the drag coefficient is lower than in the subcritical regime (thinner boundary layer with a separation point further downstream).

In Fig. 2, $\mathcal{P}(C_{L_e})$ for Post case shows a smaller dispersion. The amplitude of lift fluctuation is also smaller (lower mode, or maximum of $\mathcal{P}(C_{L_e})$), leading to a smaller C_L'. Physically, the thinner boundary layer and smaller turbulent vortices in the wake induce lower variation in the pressure distribution and so the lift fluctuation. For the three regimes, the fact that this envelope C_{L_e} is far from a Dirac function is part of the motivation of this work. The robustness of the proposed identification procedure for generalized vortex shedding model will be illustrated in the following using statistics of the lift and its envelope.

3. Derivation of a generalized model

A new model is presented here. It differs from existing models because it is based on the experimental data at high frequency (or fast dynamic) while existing models are phenomenological (Krenk and Nielsen, 1999; Hartlen and Currie, 1970; Facchinetti et al., 2004) or based on some physical arguments (Tamura, 1981). By basing the proposed model on the fast dynamics of experimental data, we can better capture the specific features of vortex shedding. This model is obtained by fitting the parameters of a non-linear model to the experimental data. The randomness observed in the experiments, in particular as to the random lift envelope, will be tackled in a second step.

3.1. Deterministic part of the model

The considered model (6) is a generalization of the existing models and is recalled here for convenience,

$$\ddot{q} + q = F(q, \dot{q}) = \dot{q}(\alpha q^2 + \beta q\dot{q} + \gamma \dot{q}^2 + \delta). \tag{7}$$

It is also general in the sense that it combines all possible odd non-linear terms of the oscillator using cubic terms that contain powers of $\dot{q}$ (*i.e.* $q^2\dot{q}$, $q\dot{q}^2$, $\dot{q}^3$) and a linear term in $\dot{q}$. Quadratic terms, like $\dot{q}^2$, would not participate to the dynamics of the wake-oscillator at leading order (first harmonic), see Appendix A. These even order terms are therefore omitted from the model.

The identification method is based on a phase portrait analysis of the observed lift. It consists in adjusting coefficients $\boldsymbol{\pi} = (\alpha, \beta, \gamma, \delta)$ from experimental measurements of the fluid variable $q(t)$ (derived from the lift coefficient, $q = 2C_L/C_{L0}$), following these steps :

1. Compute $\dot{q}$ and q̈ from q (using finite differences) to obtain and represent the experimental trajectories of $\ddot{q} + q$ as a function of q and $\dot{q}$.
2. Adjust and fit the polynomial surface $F(q, \dot{q})$ on experimental (non-parametric) trajectories of $Q_{ij}^* = (\ddot{q} + q)_{(q_i, \dot{q}_j)}$ measured for n_p values of q and $\dot{q}$, using a least-square fitting procedure, to identify model coefficients $\alpha, \beta, \gamma, \delta$

$$\hat{\boldsymbol{\pi}} = \arg\min_{\boldsymbol{\pi}} \sum_{i,j}^{n_p} \left(F(q_i, \dot{q}_j; \boldsymbol{\pi}) - Q_{ij}^*\right)^2 \tag{8}$$

where $F(q_i, \dot{q}_j; \boldsymbol{\pi})$ is given by Eq. (7). This procedure is illustrated in Fig. 3, with (1) the experimental trajectories of $\ddot{q} + q$ as a function of $(q, \dot{q})$ and (2) the surface fitting using additional constraints developed below.

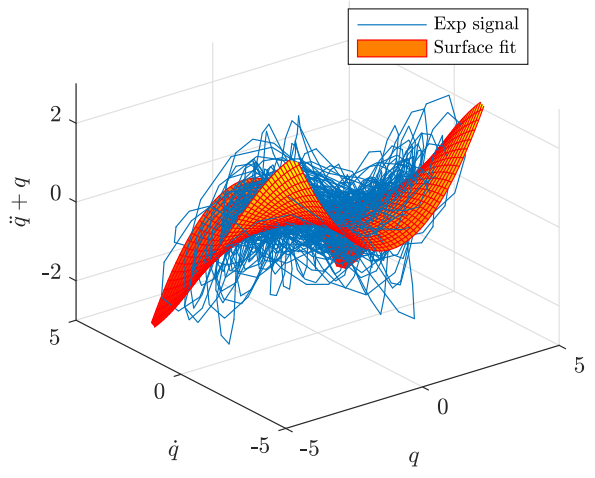

Fig. 3. (a) Experimental trajectories of $\ddot{q}+q$ and deterministic polynomial surface fitting of $F(q,\dot{q})$ in phase spaces.

Using a harmonic balance procedure, it is possible to add some constraints on coefficients in order to improve the identification robustness to match the expected limit cycle amplitude (see Appendix A). It is shown that the term in $q\dot{q}^2$ does not contribute to the amplitude of the limit cycle and therefore $\beta = 0$ is chosen. From experimental measurements, the identification procedure without constraints on $\alpha, \beta, \gamma, \delta$ returns negligible values for β compared to the other coefficients. The remaining constraint is,

$$\frac{Q^2}{4}(\alpha + 3\gamma) + \delta = 0. \tag{9}$$

with the limit cycle amplitude $Q \neq 0$. This equation also gives a constraint on coefficients for a given limit cycle amplitude, $Q = 2$ in order to be consistent with the definition of q and recover the physical lift coefficient amplitude $\tilde{C}_L = \frac{C_{L0}}{2} Q = C_{L0}$ (consistent with the limit cycle amplitude of Van der Pol oscillator), Eq. (9) becoming $\alpha + 3\gamma + \delta = 0$. The limit cycle amplitude $Q = 2$ is consistent with the one for a Van der Pol oscillator (Hagedorn and Stadler, 1988).

Another constraint on coefficients comes from a stability analysis : in order to have a non-zero limit cycle, the state space equation needs to be unstable at the origin $x = (q, \dot{q}) = (0, 0) = p$, otherwise $(q, \dot{q})$ would stay at this fixed point p. The corresponding autonomous of Eq. (7) can be written in the form $\dot{\underline{q}} = \underline{c}(\underline{x})$ (see details in Appendix A). Using the Hartman–Grobman theorem, the stability can be assessed using the Jacobian matrix $J_p(v)$ of the vector field $\underline{v}$ at the fixed point p : the solution is asymptotically stable if all eigenvalues of J have strictly negative real part. In Appendix A, eigenvalues of J are computed and a discussion on the influence of the sign of δ allows to conclude that the solution is unstable for $\delta > 0$. To conclude, the optimization problem (8) is solved under the constraints:

$$\delta = -(\alpha + 3\gamma) > 0. \tag{10}$$

Fig. 3 illustrates the result of the complete fitting procedure for Sub1 case using the constraints on model coefficients. The overall shape of the non-linearity is correctly captured by the polynomial surface fit but a residual is observed between the experimental trajectories and the deterministic surface. Fig. 4 illustrates this normalized residual $R = \ddot{q}+q-F(q,\dot{q})/\sigma_q$ (with σ_q the rms of q) in the $(q, \dot{q})$ plane. Residuals are equally distributed around 0, showing that the parametric shape of the model seems to be appropriate. Furthermore, the PSD of the residual will be used to inspire the stochastic model for the additive noise. Fig. 5 shows the PSD of the residual R, experimental lift q, acceleration $\ddot{q}$, the left handside of Eq. (6) $\ddot{q}+q$. Most energy of lift coefficient q is located around f_0. The acceleration $\ddot{q}$ shows also energy content at $3f_0$, justifying also the use of third order terms in the non-linear model. The shape of the residual spectrum is flat in the low frequency range, without dominant frequency, and linear in log–log scales as frequency reaches large values, showing an appropriate parametric model. However, the observed variation amplitude of $\pm 0.6\sigma_q$ in Fig. 4 are non negligible and this residual can be seen as an additive noise. This observation justifies the need to add a stochastic term in the model, developed in the following.

Finally, the procedure for the deterministic part of the model can be applied to the three regimes. Obtained values of α, γ, δ are summarized in Table 3.

3.2. Additive noise

As discussed in the introduction and observed in the previous section, the lift coefficient measured on a static circular cylinder is not perfectly harmonic. Models (2), which are based on a Van der Pol or Rayleigh equation, result in periodic or

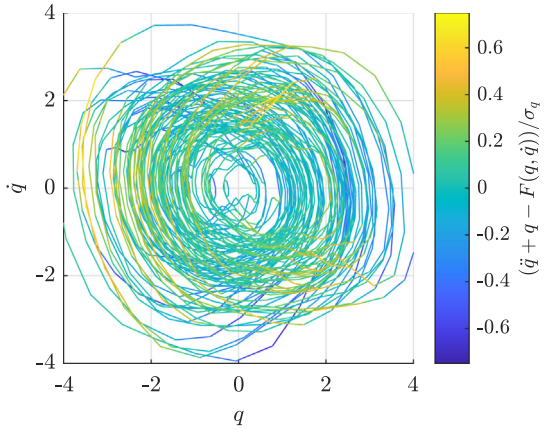

Fig. 4. Residual between experimental trajectories of Fig. 3 and deterministic fitted surface.

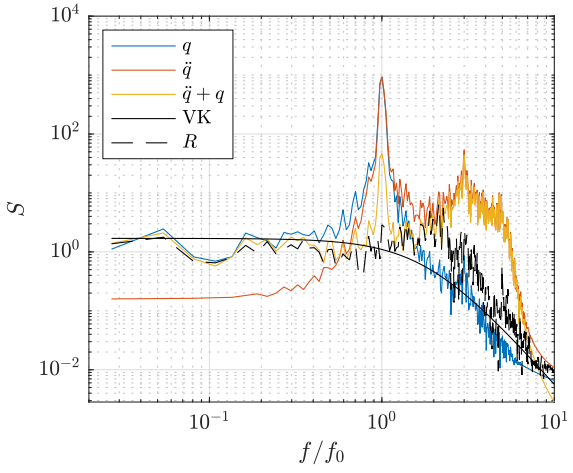

Fig. 5. Spectrum of residual R, experimental lift q, acceleration $\ddot{q}$, $\ddot{q}+q$ and von Karman type.

Table 3
Identified coefficients of the generalized model for the three regimes.

Regime	α	γ	δ
Sub1	−0.085	0.009	0.057
Sub2	−0.078	0.009	0.051
Post	−0.016	0.002	0.011

quasi-periodic solutions depending on the range of parameters (Glendinning et al., 1994). In their original deterministic formulations, they are not capable of emulating a chaotic envelope as observed in experimental data. One way to obtain a chaotic envelope with a Van der Pol model (or similar) is to use time varying coefficients in the form of a stochastic parametric loading., see e.g. Denoël (2020). This modelling option is particularly well suited when it is possible to justify that some parameters of the wake-oscillator model, e.g. $U + u(t)$, do vary in time. Evoking a quasi-steady theory, this offers a straightforward manner to model turbulent flows (Denoël, 2020). This option is not followed in this paper which considers uniform flows. Instead, noise is added in the model as a right hand-side in the generalized Van der Pol equation, which is assumed to better correspond to modelling the wake turbulence creating the slow fluctuations of the lift envelope.

In models (2), such as the Vickery–Basu model, the way of modelling the stochastic nature of vortex shedding is substantially different. Indeed, the lift force created by vortex shedding is directly represented by its power spectral density and not as the solution of a differential equation.

A first possibility is to use the lift spectrum S_{C_L} (Power Spectral Density (PSD)) proposed by Basu and Vickery (1983), which was found to fit quite well experimental data (King, 1977). In fact, Vickery and Clark (1972) followed a similar

approach by proposing,

$$S_{C_L}(f) = \frac{\tilde{C}_L^2}{\sqrt{\pi} B f_0} e^{-\left(\frac{1-\frac{f}{f_0}}{\frac{B}{f_0}}\right)^2} \tag{11}$$

where f is the frequency and B the bandwidth, a measure of the spread of the lift spectrum. In the absence of turbulence in the oncoming flow, the bandwidth $B = (B_0^2 + 2(\sigma_u/U_\infty)^2)^{1/2}$ is reduced to B_0 which has typical values in the range 0.05–0.1 (Basu and Vickery, 1983). The formulation of Eq. (11) is consistent with experimental observations around f_0, the vortex shedding frequency. However as illustrated next, the spectrum at other frequencies, slightly away from this narrow frequency band, does not match experimental data. This fact is illustrated in Section 4, with a comparison of models results. This is not a real drawback of the model, since the purpose of the Vickery–Basu model is to provide an equivalent loading that yields the same response, but not necessarily i.e. not the same lift along the whole frequency domain.

In summary, models (2) are now mostly deterministic (or in a parametric stochastic form that is not appropriate for uniform flows) while models (1) are exclusively stochastic. Models (2), when embedded in the 2-DOF model are able to capture the self-limiting nature of vortex induced vibrations. Conversely, models (1) are better suited to the forced response at high Scruton (Piccardo and Solari, 1998) and do not offer the adaptive nature of the loading as a function of the amplitude of the body. Equivalent damping models (Lupi et al., 2018) use a forced feedback with the lift force that depends on the state (amplitude) of the structural oscillator but the particular dynamics of the lift force is not modelled by a fluid equation.

With the perspectives of deriving a model offering the advantages of the two (traditionally opposed) approaches, we suggest to introduce an additive forcing noise $\eta(t)$ to Eq. (7), to obtain the final form of the model :

$$\ddot{q} + q = F(q, \dot{q}) + \eta \tag{12}$$

As detailed next, the proposed form of $F(q, \dot{q})$ is an extension of the non-linear terms in a Van der Pol equation. It is important to notice that several studies (Zhu and Yu, 1987; Belousov et al., 2020) have focused on the influence of a white noise excitation to Van der Pol equation. Nevertheless, we found that this kind of broadband forcing would create a lift force $q(t)$ which does not match experiments, as illustrated in Section 4. Indeed, we infer that the stochasticity that appears in the lift force even in smooth flow comes from the signature of the downstream flow as a wake turbulence. If a parallel with $\eta(t)$ could be made, it is clear that its frequency content cannot be a white noise, which solely remains a mathematical conceptualization. With this in mind, other types of noise were investigated in our study. Among several choices for the modelling of $\eta(t)$ (such as an Ornstein–Uhlenbeck process or other turbulence processes), consideration of a Von Karman-type spectrum has shown very accurate results. Interestingly this spectrum is consistent with the Kolmogorov cascade with a slope in $1/\omega^{5/3}$ at higher frequencies. Its appropriateness could be explained by the fact that the stochasticity in the observations is a result of the wake turbulence. Even if this seems to introduce a rationale in considering a Von Karman spectrum, it should be kept in mind that this additive noise does not represent the physical quantity directly (i.e. the pressure or its resultant). It is rather a mathematical tool added as a random entry to the generalized Van der Pol model that fulfils the objectives we are trying to achieve: to reproduce statistics of the experimental lift. It is therefore proposed to model the random process $\eta(t)$ as a zero-mean Gaussian process with a power spectral density expressed as,

$$\Phi_\eta(\omega) = \sigma_\eta^2 \frac{2L_\eta}{\pi U_\infty} \frac{1}{\left(1 + \left(1.339 L_\eta \frac{\omega}{U_\infty}\right)^2\right)^{\frac{5}{6}}} \tag{13}$$

with σ_η the standard deviation of the additive noise and L_η a parameter linked to its characteristic time (i.e. as L_η increases, the dynamics in η is slower, the characteristic frequency decreases). Conversly, the Von Karman spectrum in Eq. (13) tends to a white noise when L_η tends to 0. An example of this PSD is presented in Fig. 5. It is a simple parametric expression that fits the PSD of the residual. Parameters of VK could be determined in order to reproduce the transition point to the inertial zone and the level in the input zone (energy production range) of VK spectrum. However, we propose a more rigorous approach. Once the deterministic coefficients of $F(q, \dot{q})$ are fitted following the procedure of Section 3.1, Von Karman parameters $\pi_{VK} = (\sigma_\eta, L_\eta)$ are determined to adjust the lift envelope shape of the model to the experimental one. This was performed by minimizing the difference between the PDF of the generated lift envelope from the model and a non-parametric estimate $\tilde{\mathcal{P}}_{C_{L_e}}$ of the PDF of the lift envelope from the experimental data, as well as the difference between the generated PSD of the lift and a non parametric estimate from experimental data $\tilde{S}_{C_L,f_i}$:

$$\hat{\boldsymbol{\pi}}_{VK} = \arg\min_{\boldsymbol{\pi}_{VK}} w_1 \sum_i^{n_b} \left(\mathcal{P}_{C_{L_e}}(q_{e,i}; \boldsymbol{\pi}_{VK}) - \tilde{\mathcal{P}}_{C_{L_e},i}\right)^2 + w_2 \sum_i^{n_f} \frac{\Delta f}{\sigma_{C_L}^2} \left(S_{C_L}(f_i; \boldsymbol{\pi}_{VK}) - \tilde{S}_{C_L,f_i}\right)^2 \tag{14}$$

with $w_1 = w_2 = 1/2$, the relative weights in the objective function. The difference of PSD has been scaled to get rid of spectrum dimensions, with the frequency step Δf and the variances of experimental lift envelope $\sigma_{C_{L_e}}^2$, $n_b = 50$ is the number of bins used to compute the PDF and n_f the number of frequencies for the PSD. More precisely, for a given value of π_{VK},

Table 4
Identified parameters of the exogenous noise.

Regime	σ_u	L_u
Sub1	0.55	1.15
Sub2	0.6	0.9
Post	0.2	1.2

1. We generate a sample of the noise $\eta(t)$ from its spectrum Eq. (13),
2. We solve the complete differential equation of the model Eq. (12) to obtain the lift force, then we compute the PDF of its envelope $\mathcal{P}_{C_{L_e}}(q_{e,i})$ as well as the PSD of the lift $S_{C_L}(f, \pi_{VK})$.
3. Ultimately the objective function to be minimized, see Eq. (14) is computed.

The purpose of the identification procedure is to generate a model whose results are close to experimental values. In conclusion, the study is made gradually, by adding a noise η on the deterministic adjusted model $F(q, \dot{q})$. The following section will illustrate the comparison of experimental data with the present model (using Von Karman and white noise spectrum), Basu's and Tamura's results.

4. Results of model prediction

The identification methodology detailed in the previous section is applied to wind tunnel data sets presented in Section 2. The identified coefficients $\boldsymbol{\pi} = (\alpha, \beta, \delta)$ and exogenous noise parameters σ_u, L_u are summarized respectively in Tables 3 and 4 for the various flow regimes considered. These specific values of the model parameters can then be used to generate time series of the lift coefficient time. These signals and the corresponding phase portrait can be compared to the experimental data. For Sub1 case (smooth surface cylinder at $Re = 4.5 \cdot 10^4$), Fig. 6 shows that the present model is able to capture correctly the experimental dynamics. The experimental window is a narrow-band process and the apparent phase shift in the time series depends on the initial condition used in the simulations, which are clearly different from those of the experimental data. So the eye should not be guided by the comparison of phases in the time series but well by the magnitude of the oscillations. Indeed, in the model, the stationary response only is considered. Both the time signal amplitude and the phase portrait dynamics are well captured by the present model. Tamura's model is also represented, a Van der Pol equation ($\boldsymbol{\pi} = (-\varepsilon_T, 0, \varepsilon_T)$) with $\varepsilon_T = 2\xi_f = 0.076$ (Tamura, 1981). As it is deterministic, the lift envelope is constant in the steady-state regime and the limit cycle amplitude is $Q = 2$. The phase portrait shape is indeed not perfectly elliptical because of the non-linearity but its shape is different from the experimental one, which exhibit significant deviations from a periodic response. The lift expression proposed by Basu and Vickery (1983) is also represented for comparison. Its parameters of bandwidth B_0 and amplitude $\tilde{C}_L$ are adjusted to experimental data. The variability and shape of the phase portrait is captured but is has a circular shape with only small variation (one harmonic) compared to experimental data. Indeed, it just corresponds to a narrowband Gaussian noise; no governing equation is solved in this case.

On Fig. 7, the five results are compared (experimental data, present model, Tamura's model, Vickery–Basu's model and the present model with a white noise forcing) for 3 data sets : Sub1, Sub2 and Post. Results are presented with four major statistics of the lift coefficients : PDF of the lift, PDF of the lift envelope, PSD of the lift and PSD of the lift envelope. The $-5/3$ slope is also superimposed to the PSD of the lift envelope to make the link with the additive noise from Von Karman spectrum (affecting more the slower dynamics, i.e. the envelope), consistent with the Kolmogorov cascade.

The PDFs of the lift and the lift envelope obtained with the present model match well experimental data for all data sets. Such results were expected as (i) the coefficients of the non-linear terms of the model are adjusted on 3D experimental phase portrait and (ii) the exogenous noise parameters are adjusted so that PDFs of lift and lift envelope match the experimental ones. The shape of lift PDF from Basu's model, as well as the white noise forcing, are Gaussian. The experimental one is however flatter in the neighbourhood of the origin, which is well captured by the present model. Tamura's model gives a harmonic signal, whose PDF has a U-shape as expected and does not correspond to experimental data. In the postcritical regime, lift amplitude decreases but the general PDF shape remains the same.

The PDF of the lift envelope is a Dirac function for Tamura's model (constant envelope). Basu's model gives an asymmetric PDF but with a too high skewness. The same shape with a different maximum is obtained for other Re, because Basu's model has only one parameter B. Using a white noise leads to a symmetric lift envelope PDF but with a too high and sharp maximum value of the PDF because of its broadband frequency content (random noise around the constant amplitude). Again, the proposed model matches very well experimental data.

The lift PSD of Basu's model captures only frequencies close to f_0. Tamura's model has only one peak at f_0. The present model with white noise is able to capture a frequency content outside the range around f_0 but the slope for higher frequencies does not match experiments. The lift PSD with the present model with a Von Karman spectrum is very close to the experimental one. In the PSD of the envelope $S_{C_{L_e}}$, the drop after $f/f_0 = 1$ is a numeric artifact of the envelope computation and the higher frequency content is not physical (the envelope of the lift is computed with a Hilbert transform and this arbitrary choice does not offer an accurate estimate of the frequency content beyond $f = f_0$).

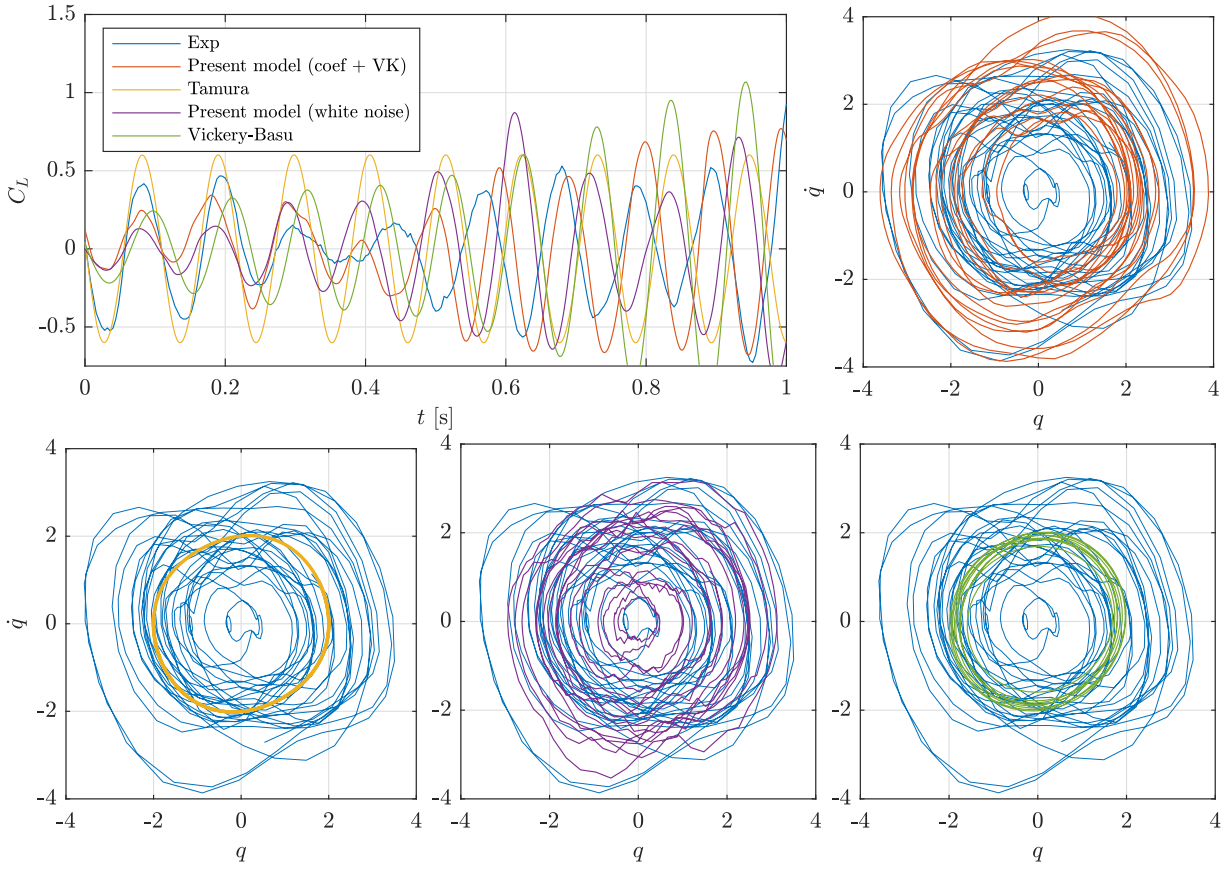

Fig. 6. Comparison Sub1 case of experimental measurements (Section 2, Table 2), present model prediction with $(\alpha, \gamma, \delta, \sigma_\eta, L_\eta) = (-0.085, 0.009, 0.057, 0.4, 1.15)$ (Section 3.1, Eq. (7) and Section 3.2, Eq. (13)), Tamura's model with $\varepsilon_T = 0.076$ (Section 1, Eq. (1)) and Vickery–Basu's model with $B_0 = 0.05$ (Section 3.2, Eq. (11)) : lift coefficient C_L and its corresponding phase portrait $(q, \dot{q})$.

The present model captures correctly the shape of $S_{C_{L_e}}$ for each data set, close to the slope in $1/\omega^{5/3}$, while predictions of Basu's model are different as soon as one gets away from the shedding frequency. The present model with white noise gives an envelope spectrum close to the experimental one but is too straight for low frequency compared to the present model with a Von Karman spectrum.

5. Discussion

The identification of coefficients has been performed using the methodology described in Section 3.1, using the whole available time signal presented in Section 2. To validate and assess the robustness of the identification, the same methodology has been applied to the two halves of the initial signal and the identified coefficients are close to those identified on the whole signal Training sets of different sizes were also investigated to cross-validate on test sets with accurate results for this application. The obtained coefficients $\alpha, \beta, \gamma, \delta$ have been obtained with the data collected in a single Wind Tunnel Laboratory. Cross-validation with experimental results coming from other wind tunnel tests is not appropriate. Indeed, there would be more variability between results obtained with different setup conditions in the same lab or from lab to lab than the residual variability in results for the same present setup. To quantify the residual variability, the objective function (Eq. (B.1)) can be interpreted as a coefficient of variation as it is computed with the mean squared error on standardized statistics (PDF and nondimensional PSD). It is equal to around 3%. The variability of results from different setups and different labs can be computed with data of Fig. 11 (lift fluctuation from the literature). For subcritical regime, the variability of C_L' (standard deviation over mean) is around 10%. This major difference indicates that the proposed methodology is just a method to identify the coefficient of a particular test setup and a particular specimen. It can just be used in the scope of the least-squares formulation (Eq. (8)) without the pretension to attempt at universal numbers. However, the model is sufficiently versatile and could be used to determine the parameters of a generalized vortex shedding model, e.g. on an ellipse or other cross-section shapes.

The first methodology presented in the paper with sequential identification is based on the fact that the time signature is different for the deterministic and the stochastic parts of the model : (1) the 3 identified coefficients $\boldsymbol{\pi} = (\alpha, \gamma, \delta)$

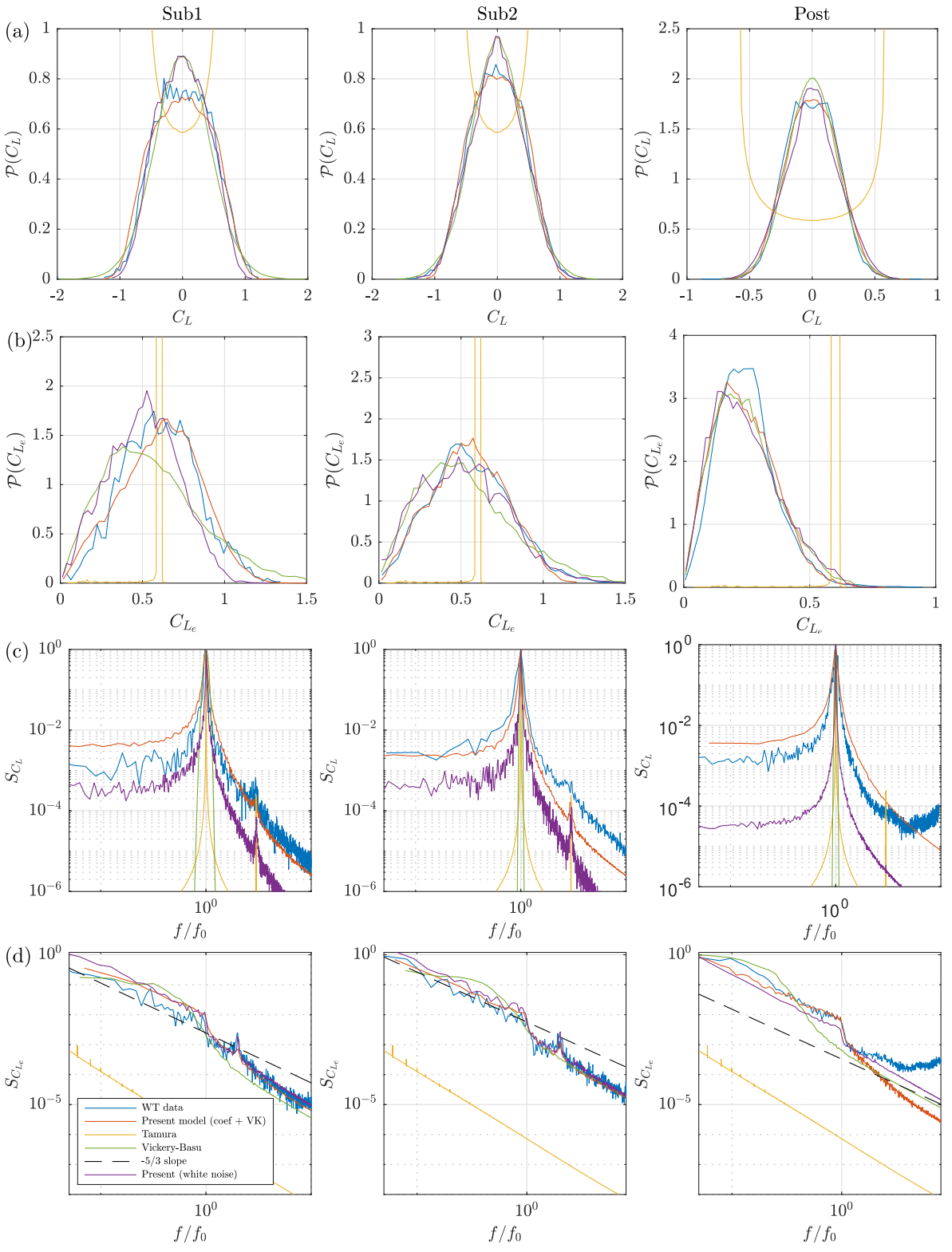

Fig. 7. Comparison between experimental measurements, present model prediction, Tamura's and Vickery–Basu's results in sub- and postcritical regimes: (a) PDF of lift coefficient, (b) PDF of lift envelope, (c) PSD of lift coefficient and (d) PSD of lift envelope. Columns correspond to the three regimes presented in Table 2 (Sub1, Sub2, Post).

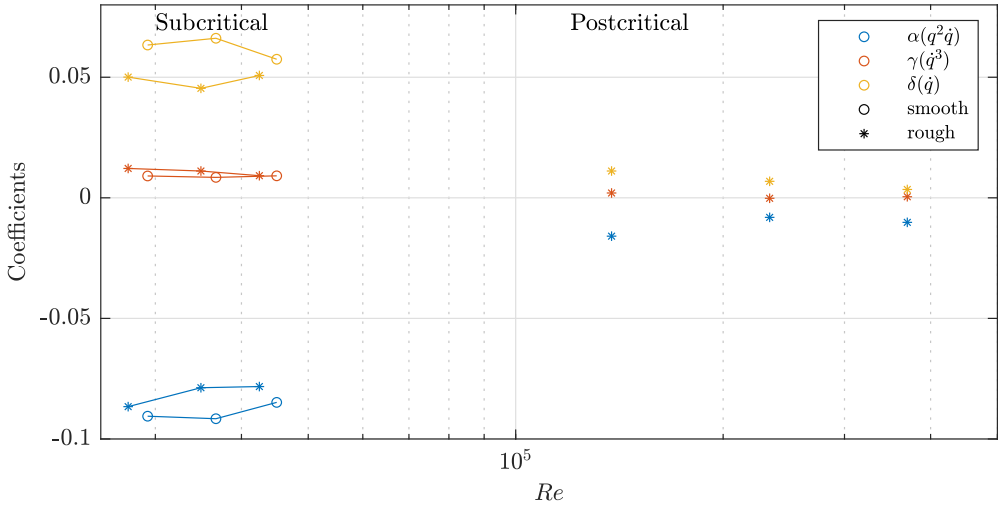

Fig. 8. Coefficients of non-linear term (α, γ, δ) adjusted from experimental measurements, as a function of Reynolds number for smooth and rough cylinder.

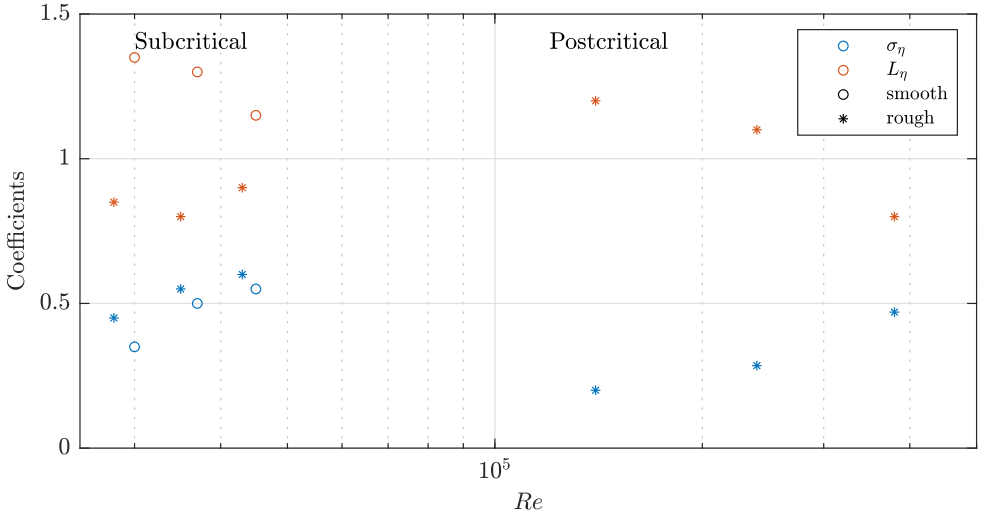

Fig. 9. Parameters used in the additional noise $\eta(t)$ as a function of Reynolds number for smooth and rough cylinder.

are associated to the slow dynamics of the deterministic model and (2) the 2 VK parameters $\boldsymbol{\pi}_{VK} = (\sigma_\eta, L_\eta)$ with the fast fluctuations from wake turbulence. A second methodology has been investigated and is presented in Appendix B. It is based on a simultaneous fit of all 5 parameters on experimental lift statistics with a 4-term objective function. The obtained results are presented in Appendix B and are very similar to the first methodology.

Fig. 8 shows the identified model coefficients $\boldsymbol{\pi} = (\alpha, \gamma, \delta)$ across regimes. In the subcritical regime (Sub1 and Sub2), they are almost Reynolds independent. The surface roughness has a small influence on the value of the coefficients (about 10% smaller in absolute value for the rough surface (Sub2)). Compared to Tamura's model parameter, α is not exactly equal to $-\delta$, because an additional term in $\dot{q}^2$ (γ) participates in the dynamics. In postcritical conditions (Post), values of model coefficients decrease and so the importance of non-linear terms in the generalized model. Parameters of the additive noise (σ_η, L_η) are reported in Fig. 9 for all regimes. For Sub1 and Sub2, these parameters are similar and σ_η is slightly higher for Sub2 because the observed lift envelope dispersion was slightly wider for rough surface case. Length scales L_η are lower for Sub2 than those for Sub1, leading to higher characteristic frequencies of turbulence in the boundary layer and wake. This could be attributed to roughness effects. For the postcritical regime, the magnitude of the fluctuations of the additive noise σ_η is lower than those in subcritical regime, which is consistent with the observation of a lower lift envelope dispersion in postcritical regime.

Note that the condition of the unstable nature of the origin, to obtain a limit cycle (Eq. (10)) gives a combination for parameters and they have to be taken as a whole. Each parameter taken independently does not characterize alone the

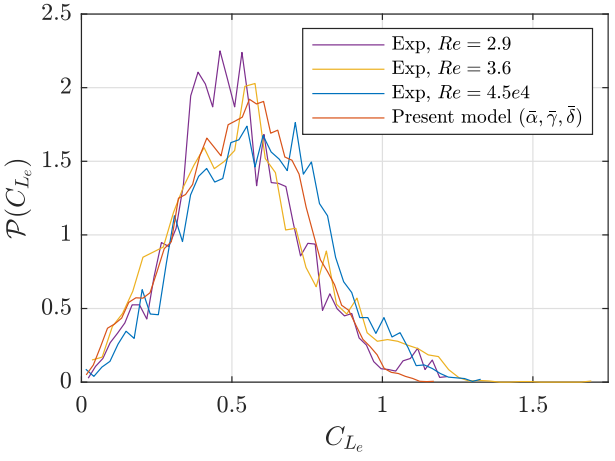

Fig. 10. Comparison of PDF of experimental lift in subcritical regime with the PDF generated with the present model (coefficients of Eq. (15)).

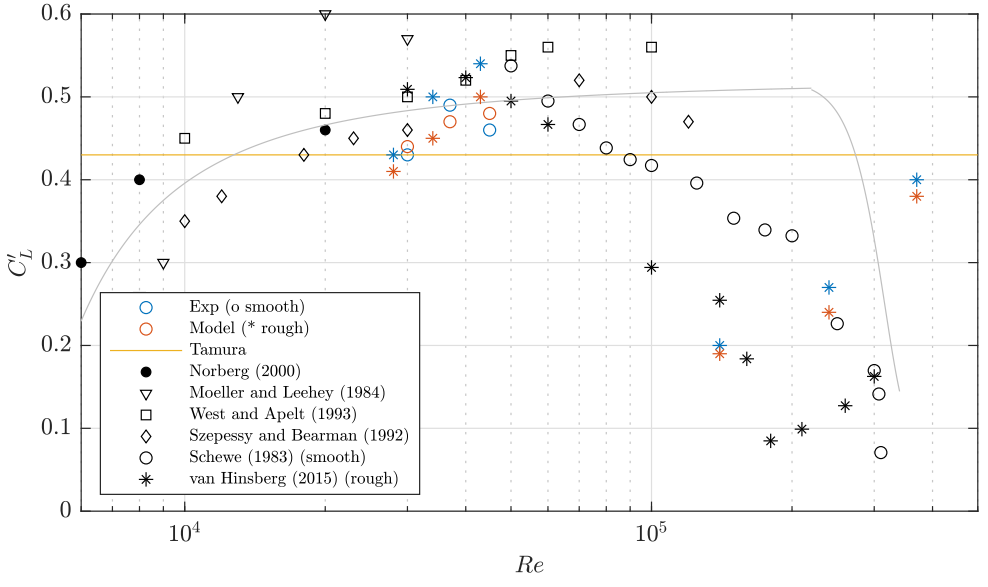

Fig. 11. Lift fluctuation, experiments vs model prediction and comparison with literature (Moeller, 1984; West and Apelt, 1993; Szepessy and Bearman, 1992; Schewe, 1983; van Hinsberg, 2015) (the grey line is an empirical trend from Norberg, 2003).

properties of the system. Values of parameters can be taken to identify the dynamics of lift coefficient in subcritical range (Sub1) for example. The purpose of this methodology paper is not to guess a physical explanation for all parameters as done in Tamura's model (Tamura, 1981) but a methodology for the generalization of non-linear model for the lift force. It is then difficult to give a physical meaning to the parameters because of their combination, they have a meaning when taken as a whole.

Some insights from the discussion can be gained: its has been shown that in the subcritical regime, model parameters are almost Reynolds independent. A final fixed set of values for $\boldsymbol{\pi}$ can then be used for different Re in this subcritical regime

$$\bar{\alpha} = -0.09, \ \bar{\gamma} = 0.009, \ \bar{\delta} = 0.063 \tag{15}$$

Fig. 10 compares the PDF of experimental lift envelope in subcritical range with the one obtained with the present model and coefficients of Eq. (15). This set of coefficients is able to capture the statistics of lift and can be used to predict the dynamics of the lift as well as the lift fluctuation C'_L. An extensive review of flow around circular cylinders was made by Norberg (2003), allowing to compare the results of the present model and experiments from the literature. Fig. 11 compares these results in term of lift fluctuation. This global quantity is a robust point of comparison to assess the accuracy of the present model. The predictions of values of C'_L obtained with the proposed model are consistent with results from

the literature in the subcritical regime, for smooth and rough cylinder surface, in low turbulence flow ($I_u < 0.2\%$). In subcritical regime, different lift fluctuation coefficients are reported (from 0.2 to 0.6), as discussed by Tamura (1981). In his model, he suggested a value of C_L' between 0.4 and 0.5 (considering an amplitude $C_{L0} = 0.6$ and a monoharmonic signal, $C_L' = C_{L0}/\sqrt{2} = 0.42$). These results are consistent around $Re = 3 \cdot 10^4$ but underestimate C_L' at higher Re, while the present model is very close to experimental results from the literature up to $Re = 5 \cdot 10^4$. The drag crisis (drop of the drag coefficient C_D) happens at $Re = 2 \cdot 10^5$ for a smooth surface cylinder and this change of regime is also observable in the variation of C_L' with Re. van Hinsberg (2015) studied the effect of roughness on regimes, with $k/D = 10^{-3}$. The onset of the critical regime appears at a lower Re (around $Re = 10^5$) than in the smooth surface case, with higher values for C_L' in postcritical regime. The value of lift fluctuation C_L' in postcritical conditions is higher when the cylinder surface roughness increases (C_L' around 0.15 for $k/D = 10^{-3}$ and $C_L' < 0.5$ for $k/D = 10^{-5}$). The cylinder surface roughness of the WT model used for the present model illustration is even higher ($k/D = 7 \cdot 10^{-3}$). The change of regime appears at an even lower Re compared to results of van Hinsberg (2015). This is consistent with results of Güven et al. (1980), Achenbach and Heinecke (1981), who showed a drag crisis starting around $Re = 8 \cdot 10^4$ for $k/D = 7 \cdot 10^{-3}$ and C_D value in the postcritical regime increases also with k/D. The same behaviour is expected for lift fluctuation C_L', which explains that present experimental measurements and model results exhibit higher C_L' for higher k/D : at $Re = 2.5 \cdot 10^5$, $C_L' = 0.23$ for $k/D = 7 \cdot 10^{-3}$, $C_L' = 0.15$ for $k/D = 2 \cdot 10^{-3}$ (Batham, 1973) and $C_L' = 0.12$ for $k/D = 2 \cdot 10^{-3}$ (van Hinsberg, 2015)). These results show that the present model is able to correctly estimate C_L' of the circular static cylinder in different regimes and can be used in a prediction phase.

6. Conclusion

The objective of this paper is to derive and analyse a generalized model of the lift force under vortex shedding around a static cylinder. Experiments show that the statistical distributions of C_L and C_{L_e} are not a Dirac-distributed, i.e. the lift is not purely mono-harmonic, as would be predicted by current wake-oscillator models. This suggested to use a spectral model in addition to an extended version of classical wake-oscillator models. Another novelty of the proposed model is that it is a wake-oscillator model, including the type of noise that is responsible for the non deterministic observations whose coefficients are obtained from specific wind tunnel testing. This paper proposes a methodology in 2 steps for the identification of lift model parameters : (i) coefficients α, γ, δ of the deterministic model and (ii) parameters of the von Karman-type exogenous noise σ_η, L_η. The deterministic part of the model (i) is a second order differential equation for the lift coefficient using a generic form for the non-linearity using all combinations odd powers of $q, \dot{q}$ up to the third degree. Coefficients of non-linear terms are adjusted on experimental dynamic trajectories thanks to a surface polynomial fit. A harmonic balance procedure and a stability analysis allows to add constraints between the coefficients. Fluctuations in the lift envelope are reproduced using an exogenous noise (ii). Parameters of the noise are adjusted using a least-square fitting of the lift envelope PDF. A second methodology has been applied, with a simultaneous fitting of all 5 model parameters on experimental lift statistics. Results are similar to the two-step procedure and proves the consistency of the method.

The procedure was applied to a circular cylinder at different Reynolds numbers and surface roughnesses. The evolution of model coefficients and Von Karman parameters with Re and roughness were studied in sub- and postcritical regimes. In the subcritical regime, model parameters are almost Reynolds independent. In the postcritical regime, non-linearities decrease with Re and additive noise from wake turbulence increases. The fluctuating lift amplitude computed from generated signal of the model were compared to experimental data. They have been found to match results from the literature for a wide range of Reynolds number. Parameters are constant in subcritical range. We suggest to use: $\bar{\alpha} = -0.09, \bar{\gamma} = 0.009, \bar{\delta} = 0.063$.

This work opens several perspectives. Among others, it offers a simple and robust way to identify non-linear coefficients in the vortex shedding model for a static circular cylinder, together with the additive noise intensity and characteristic time. This study represents the starting point for two upcoming extensions. First, static cylinders arranged in tandem configuration could benefit from this type of model, which is supposed to be a better stating point than other models capturing the slow dynamics only. Indeed, as soon as the interaction of two cylinders in considered, the interacting fast dynamics need to be modelled accurately. Second, this equation, combined with a structural one, can be used to model cylinders in free vibration with carefully adapted coupling terms (assuming a one degree of freedom VIV). This extension is not trivial but is in current study. Starting from the second methodology presented in the paper (simultaneous fitting of all 5 model parameters),two coupling terms can be added for lift and structure equations and all 7 coefficients can be adjusted simultaneously using experimental lift and structural displacement statistics. Finally, by doubling the two-equation system, the extension to flexible cylinders in tandem arrangement is also possible.

CRediT authorship contribution statement

François Rigo: Conceptualization, Methodology, Software, Data curation, Writing, Visualization, Investigation, Validation. **Thomas Andrianne:** Conceptualization, Methodology, Writing, Visualization, Supervision, Validation, Reviewing and editing. **Vincent Denoël:** Conceptualization, Methodology, Writing, Visualization, Supervision, Validation, Reviewing and editing.

Declaration of competing interest

The authors declare that they have no known competing financial interests or personal relationships that could have appeared to influence the work reported in this paper.

Data availability

Data will be made available on request.

Acknowledgement

The authors want to thank the Belgian National Fund for Scientific Research (FNRS) for their support.

Appendix A. Fitting method constraints

A.1. Harmonic balance

The harmonic balance procedure consists to substitute the Ansatz for the wake variable $q(t) \approx q_h(t) = Q_c \cos\omega t + Q_s \sin\omega t$ in Eq. (7), after computing $\dot{q}_h, \ddot{q}_h$ and non-linear terms $q_h^2\dot{q}_h, q_h\dot{q}_h^2, \dot{q}^3$ thanks to trigonometric identities of third order.

$$\begin{aligned}
&\left[(1-\omega^2)Q_c - \frac{\alpha\omega}{4}(Q_c^2Q_s + Q_s^3) - \frac{\beta\omega^2}{4}(Q_c^3 + Q_cQ_s^2) - \frac{3\gamma\omega^3}{4}(Q_s^3 + Q_c^2Q_s) - \delta\omega Q_s\right]\cos\omega t \\
&+\left[(1-\omega^2)Q_s + \frac{\alpha\omega}{4}(Q_c^3 + Q_cQ_s^2) - \frac{\beta\omega^2}{4}(Q_s^3 + Q_c^2Q_s) + \frac{3\gamma\omega^3}{4}(Q_c^3 + Q_cQ_s^2) + \delta\omega Q_c\right]\sin\omega t \\
&+\left[\frac{\alpha\omega}{4}(Q_s^3 - 3Q_c^2Q_s) + \frac{\beta\omega^2}{4}(Q_c^3 - 3Q_cQ_s^2) + \frac{\gamma\omega^3}{4}(3Q_c^2Q_s - Q_s^3)\right]\cos 3\omega t \\
&+\left[\frac{\alpha\omega}{4}(Q_c^3 - 3Q_cQ_s^2) + \frac{\beta\omega^2}{4}(3Q_c^2Q_s - Q_s^3) - \frac{3\gamma\omega^3}{4}(3Q_cQ_s^2 - Q_c^3)\right]\sin 3\omega t = 0
\end{aligned} \tag{A.1}$$

Higher harmonics are neglected ($\cos 3\omega t$ and $\sin 3\omega t$) and first harmonics are balanced,

$$R_c := (1-\omega^2)Q_c - \frac{\alpha\omega}{4}(Q_c^2Q_s + Q_s^3) - \frac{\beta\omega^2}{4}(Q_c^3 + Q_cQ_s^2) - \frac{3\gamma\omega^3}{4}(Q_s^3 + Q_c^2Q_s) + \delta\omega Q_s = 0 \tag{A.2}$$

$$R_s := (1-\omega^2)Q_s + \frac{\alpha\omega}{4}(Q_c^3 + Q_cQ_s^2) - \frac{\beta\omega^2}{4}(Q_s^3 + Q_c^2Q_s) + \frac{3\gamma\omega^3}{4}(Q_c^3 + Q_cQ_s^2) - \delta\omega Q_c = 0. \tag{A.3}$$

By transforming Q_c and Q_s to polar coordinates ($Q_c = Q\cos\theta$, $Q_s = Q\sin\theta$) and applying algebraic manipulations : $\cos\theta$(A.2)+$\sin\theta$(A.3) and $\cos\theta$(A.3)-$\sin\theta$(A.2), two relations are obtained,

$$(1-\omega^2)Q - \frac{\beta\omega^2 Q^3}{4} = 0 \tag{A.4}$$

$$\frac{\alpha\omega Q^3}{4} + \frac{3\gamma\omega^3 Q^3}{4} + \delta\omega Q = 0. \tag{A.5}$$

Notice that adding $\dot{q}^2$ in F would have produced quadratic harmonics ($\sin^2\omega t, \cos^2\omega t, \cos\omega t\sin\omega t$, associated to second harmonics $\sin 2\omega t, \cos 2\omega t$). At leading order, these even harmonics are discarded. Indeed, they do not have the quality of restoring energy, i.e. they would lead to an unstable solution. The use of ω in $q_h(t)$ was made to remain general, *i.e.* if an external force is applied to the system at this frequency ω. Nevertheless, without forcing term, the characteristic frequency of the oscillator leads to $\omega = 1$ and Eqs. (A.4)–(A.5) simplifies to (with a limit cycle amplitude $Q \neq 0$),

$$\beta = 0 \text{ and } \frac{Q^2}{4}(\alpha + 3\gamma) + \delta = 0. \tag{A.6}$$

A.2. Stability

The stability of Eq. (7) is discussed using its autonomous form

$$\dot{\underline{x}} = \underline{v}(\underline{x}), \text{ with } \underline{x} = \begin{pmatrix} q \\ \dot{q} \end{pmatrix} \text{ and } \underline{v}(\underline{x}) = \begin{pmatrix} \dot{q} \\ F(q,\dot{q}) - q \end{pmatrix} \text{ with } F = \dot{q}(\alpha q^2 + \beta q\dot{q} + \gamma\dot{q}^2 + \delta) \tag{A.7}$$

Table B.5
Comparison of model coefficients (Sub1 case) obtained from both methods.

Method	α	γ	δ	σ_η	L_η
1	−0.085	0.009	0.057	0.55	1.15
2	−0.092	0.01	0.062	0.61	1.28

Its Jacobian matrix at point $p = (0, 0)$ is,

$$J_p(v) = \left.\frac{\partial \underline{v}}{\partial \underline{x}}\right|_p = \left.\begin{pmatrix} 0 & 1 \\ -1 + \partial_q F & \partial_{\dot{q}} F \end{pmatrix}\right|_p = \begin{pmatrix} 0 & 1 \\ -1 & \delta \end{pmatrix} \tag{A.8}$$

with $\partial_q F\big|_p = (2\alpha q\dot{q} + \beta\dot{q}^2)\big|_{(0,0)} = 0$ and $\partial_{\dot{q}} F\big|_p = (\alpha q^2 + 2\beta q\dot{q} + 3\gamma\dot{q}^2 + \delta)\big|_{(0,0)} = \delta$. The eigenvalues of $J_p(v)$ are then,

$$\lambda = \frac{\delta \pm \sqrt{\delta^2 - 4}}{2}. \tag{A.9}$$

If $\delta < -2$, then $\delta \pm \sqrt{\delta^2 - 4} < 0$ and if $\delta > 2$, then $\delta \pm \sqrt{\delta^2 - 4} > 0$. If $|\delta| < 2$, λ is complex and its real part is equal to $\delta/2$, the solution is then unstable if $\mathcal{R}e(\lambda) = \delta/2 > 0$. By combining these criteria, the solution is unstable if $0 < \delta < 2$ and if $\delta > 2$, thus if $\delta > 0$.

Appendix B. Second methodology

This second methodology consists to fit simultaneously all 5 model parameters $\boldsymbol{\pi}_0 = (\alpha, \gamma, \delta, \sigma_\eta, L_\eta)$ based on lift statistics. The model is adjusted on experimental (non-parametric) PDFs and PSDs of lift and lift envelope, measured for n_b bins in PDFs and n_f frequencies for PSDs. In practice, the lift is generated by solving Eq. (12) as a function of a parameter set $\boldsymbol{\pi}_0$ and its statistics are computed (PDF et PSD of lift and lift envelope). Then, the parameters $\boldsymbol{\pi}_0$ are adjusted using a least-square fitting with a 4 terms objective function,

$$\begin{aligned}\hat{\pi}_0 = &\arg\min_{\boldsymbol{\pi}_0} w_1 \sum_i^{n_b} \left(\mathcal{P}_{C_L}(q_i;\boldsymbol{\pi}_0) - \tilde{\mathcal{P}}_{C_{L,i}}\right)^2 + w_2 \sum_i^{n_b} \left(\mathcal{P}_{C_{L_e}}(q_{e,i};\boldsymbol{\pi}_0) - \tilde{\mathcal{P}}_{C_{L_e,i}}\right)^2 \\ &+ w_3 \sum_i^{n_f} \frac{f_i \left(S_{C_L}(f_i;\boldsymbol{\pi}_0) - \tilde{S}_{C_L,f_i}\right)^2}{\sigma^2_{C_L}} + w_4 \sum_i^{n_f} \frac{f_i \left(S_{C_{L_e}}(f_i;\boldsymbol{\pi}_0) - \tilde{S}_{C_{L_e},f_i}\right)^2}{\sigma^2_{C_{L_e}}}\end{aligned} \tag{B.1}$$

with $w_i = 1/4$ the relative weights in the objective function. The differences of PSDs have been scaled by f/σ^2 to get rid of spectrum dimensions, with the frequency f and the variances of experimental lift $\sigma^2_{C_L} = C_L'^2$ and lift envelope $\sigma^2_{C_{L_e}}$. Table B.5 compares model coefficients obtained using the second method and results are similar to the first methodology.

References

Achenbach, E., Heinecke, E., 1981. On vortex shedding from smooth and rough cylinders in the range of Reynolds numbers 6×10^3 to 5×10^6. J. Fluid Mech. 109, 239–251.
Aswathy, M.S., Sarkar, Sunetra, 2019. Effect of stochastic parametric noise on vortex induced vibrations. Int. J. Mech. Sci. 153–154, 103–118.
Basu, R.I., Vickery, B.J., 1983. Across-wind vibrations of structure of circular cross-section. Part II. development of a mathematical model for full-scale application. J. Wind Eng. Ind. Aerodyn. 12 (1), 75–97.
Batham, J.P., 1973. Pressure distributions on circular cylinders at critical Reynolds numbers. J. Fluid Mech. 57 (2), 209–228.
Belousov, R., Berger, F., Hudspeth, A.J., 2020. Volterra-series approach to stochastic nonlinear dynamics: Linear response of the Van der Pol oscillator driven by white noise. Phys. Rev. E 102, 032209.
Bishop, R.E.D., Hassan, A.Y., 1964. The lift and drag forces on a circular cylinder in a flowing fluid. Proc. Royal Soc. Lond. Ser. A Math. Phys. Sci. 277 (1368), 32–50.
Collins, N.J., 1976. Transverse Forces on Smooth and Rough Cylinders in Harmonic Flow at High Reynolds Numbers. Calhoun.
Denoël, V., 2020. Derivation of a slow phase model of vortex-induced vibrations for smooth and turbulent oncoming flows. J. Fluids Struct. 99, 103145.
Dubois, R., Andrianne, T., 2022. Flow around tandem rough cylinders: Effects of spacing and flow regimes. J. Fluids Struct. 109, 103465.
Facchinetti, M., de Langre, E., Biolley, F., 2004. Coupling of structure and wake oscillators in vortex-induced vibrations. J. Fluids Struct. 19, 123–140.
Glendinning, P., Crighton, D.G., Ablowitz, M.J., Davis, S.H., Hinch, E.J., Iserles, A., Ockendon, J., Olver, P.J., 1994. Stability, instability and chaos: An introduction to the theory of nonlinear differential equations. Cambridge Texts in Applied Mathematics, Cambridge University Press.
Güven, O., Farell, C., Patel, V.C., 1980. Surface-roughness effects on the mean flow past circular cylinders. J. Fluid Mech. 98 (4), 673–701.
Hagedorn, P., Stadler, W., 1988. Non-Linear Oscillations. In: Oxford engineering science series, Clarendon Press.
Hartlen, R.T., Currie, I.G., 1970. Lift-oscillator model of vortex-induced vibration. J. Eng. Mech. Div. 96, 577–591.
Huseby, M., Grue, J., 2000. An experimental investigation of higher-harmonic wave forces on a vertical cylinder. J. Fluid Mech. 414.
King, R., 1977. A review of vortex shedding research and its application. Ocean Eng. 4 (3), 141–171.
Krenk, S., Nielsen, S.R.K., 1999. Energy balanced double oscillator model for vortex-induced vibrations. J. Eng. Mech. 125, 263–271.

Lienhard, J.H., 1966. Synopsis of Lift, Drag, and Vortex Frequency Data for Rigid Circular Cylinders. In: Bulletin Washington State University. College of Engineering. Research Division, 300, Technical Extension Service, Pullman, Wash.
Lupi, F., Niemann, H.J., Höffer, R., 2018. Aerodynamic damping model in vortex-induced vibrations for wind engineering applications. J. Wind Eng. Ind. Aerodyn. 174, 281–295.
Matlab, 2019. Version 9.7.0 (R2019b). The MathWorks Inc. Natick, Massachusetts.
Moeller, M.J., 1984. Measurement of Unsteady Forces on a Circular Cylinder in Cross Flow at Subcritical Reynolds Numbers (Ph.D. thesis). Massachusetts Institute of Technology, Dept. of Ocean Engineering.
Nielsen, S.R.K., Krenk, S., 1997. Stochastic Response of Energy Balanced Model for Vortex-Induced Vibration. In: Structural Reliability Theory, (166), Dept. of Building Technology and Structural Engineering, p. 16, Presented at ICOSSAR '97, Kyoto, Japan, November 24-28, 1997 PDF for print.
Norberg, C., 2003. Fluctuating lift on a circular cylinder: review and new measurements. J. Fluids Struct. 17 (1), 57–96.
Piccardo, G., Solari, G., 1998. Generalized equivalent spectrum technique. Wind Struct. 1, 161–174.
Schewe, G., 1983. On the force fluctuations acting on a circular cylinder in crossflow from subcritical up to transcritical Reynolds numbers. J. Fluid Mech. 133, 265–285.
So, R.M.C., Wang, X.Q., Xie, W.-C., Zhu, J., 2008. Free-stream turbulence effects on vortex-induced vibration and flow-induced force of an elastic cylinder. J. Fluids Struct. 24, 481–495.
Szepessy, S., Bearman, P.W., 1992. Aspect ratio and end plate effects on vortex shedding from a circular cylinder. J. Fluid Mech. 234, 191–217.
Tamura, Y., 1981. Wake-oscillator model of vortex-induced oscillation of circular cylinder. J. Wind Eng. 1981 (10), 13–24.
Ulveseter, J.V., Thorsen, M.J., Saevik, S., Larsen, C.M., 2017. Stochastic modelling of cross-flow vortex-induced vibrations. Mar. Struct. 56, 260–280.
van Hinsberg, N.P., 2015. The Reynolds number dependency of the steady and unsteady loading on a slightly rough circular cylinder: From subcritical up to high transcritical flow state. J. Fluids Struct. 55, 526–539.
Vickery, B.J., Basu, R.I., 1983. Across-wind vibrations of structures of circular cross-section. Part I. development of a mathematical model for two-dimensional conditions. J. Wind Eng. Ind. Aerodyn. 12 (1), 49–73.
Vickery, B.J., Clark, A.W., 1972. Lift or across-wind response of tapered stacks. J. Struct. Div. 98 (1), 1–20.
West, G.S., Apelt, C.J., 1993. Measurements of fluctuating pressures and forces on a circular cylinder in the Reynolds number range 1e4 to 2.5e5. J. Fluids Struct. 7 (3), 227–244.
Zhu, W.-Q., Yu, J.-S., 1987. On the response of the Van der Pol oscillator to white noise excitation†. J. Sound Vibr. 117 (3), 421–431.